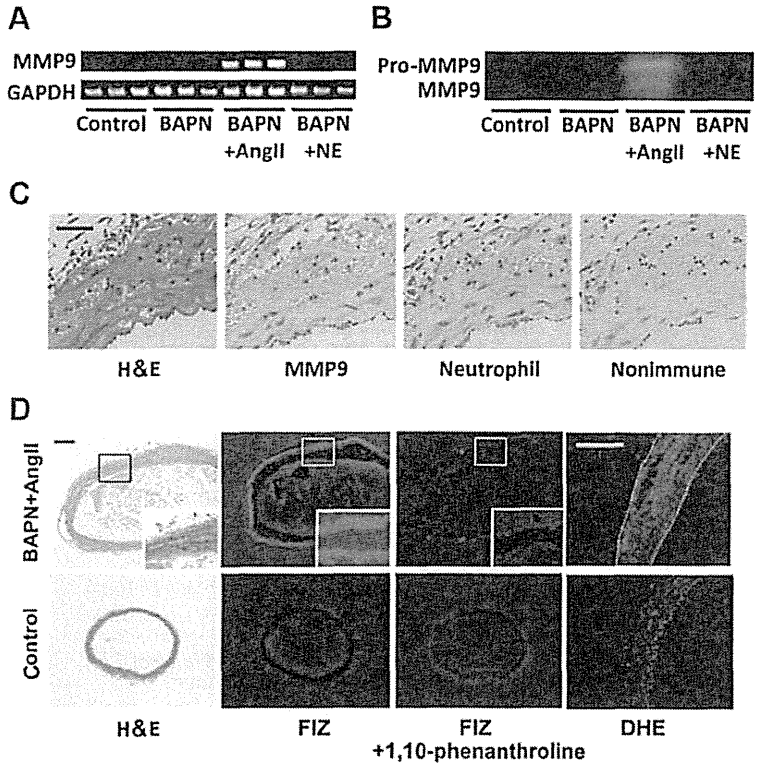

Figure 4. AAD in BAPN/AngII-treated wild type (WT) mice is accompanied by enhanced MMP9 expression, neutrophil infiltration, and superoxide production. **A**, Analysis of *MMP9* mRNA expression by reverse transcription polymerase chain reaction in aortic tissues from the WT mice treated with vehicle (control), BAPN, BAPN/AngII (BAPN+AngII), or BAPN/NE (BAPN+NE). Polymerase chain reaction products of 3 independent samples from each group are shown. **B**, Gelatinolytic activity of the aortic tissue homogenates was assessed by gelatin zymography. BAPN/AngII-treated WT aorta shows gelatinolytic bands of 92 kDa and 87 kDa, corresponding to pro-MMP9 and active MMP9, respectively. **C**, Serial paraffin sections of dissected thoracic aorta of BAPN/AngII-treated WT mice were stained with H&E and immunostained with anti-MMP9 antibody, antineutrophil antibody, or control immunoglobulin G. Note the infiltration of MMP9-positive neutrophils in the media of the dissected lesion. **D**, Film in situ zymography and dihydroethidium staining of aortic tissues from BAPN/AngII-treated or control vehicle-treated WT mice. Serial frozen sections were made and stained with H&E or subjected to film in situ zymography using gelatin films coated with or without 1,10-phenanthroline. Frozen sections were also stained with dihydroethidium. Scale bars, 200 μm. AAD indicates acute aortic dissection; BAPN, β-aminopropionitrile monofumarate; AngII, angiotensin II; WT, wild type; MMP9, matrix metalloproteinase 9; NE, norepinephrine; H&E, hematoxylin and eosin stain; FIZ, film in situ zymography; GAPDH, glyceraldehyde 3-phosphate dehydrogenase; and DHE, dihydroethidium.

thoracic aortas (Figure 5). In control mice treated with BAPN alone or BAPN and NE, immunostaining of MMP9 and neutrophils was only rarely observed in the tissues (Figure 5). These findings suggest that the increased levels of MMP9 detected in the AAD aortas are derived primarily from neutrophils that infiltrate both the aortic intima and media.

Reduction of AAD Incidence by Pharmaceutical and Genetic Depletion of MMP9 or by Neutrophil Depletion

To determine whether MMP9 plays a direct role in the AAD mouse model, BAPN/AngII-treated mice were treated with synthetic MMP inhibitor ONO-4817. As shown in Figure 6A, when ONO-4817 was administered orally on daily basis to BAPN-treated WT mice from 48 hours prior to AngII infusion until sacrifice, the incidence of AAD decreased significantly from 100% to 60%, and spontaneous death caused by aortic rupture was blocked completely. Consistent with these observations, when *MMP9*$^{-/-}$ mice were treated with BAPN/AngII, AAD incidence was attenuated remarkably to basal levels (10% of the *MMP9*$^{-/-}$ mice) whereas BAPN alone induced thoracic aneurysm formation at a frequency comparable with that observed in WT mice (Figure 6A and 6B). Hence, these findings support a direct role for MMP9 in the development of AAD.

Although multiple cell populations are capable of expressing MMP9 (eg, macrophages,[12] endothelial cells,[26] and vascular smooth muscle cells[24]), neutrophil infiltrates dominated the affected tissues. As such, we depleted neutrophils during aneurysm formation by treating the mice with anti-Gr-1

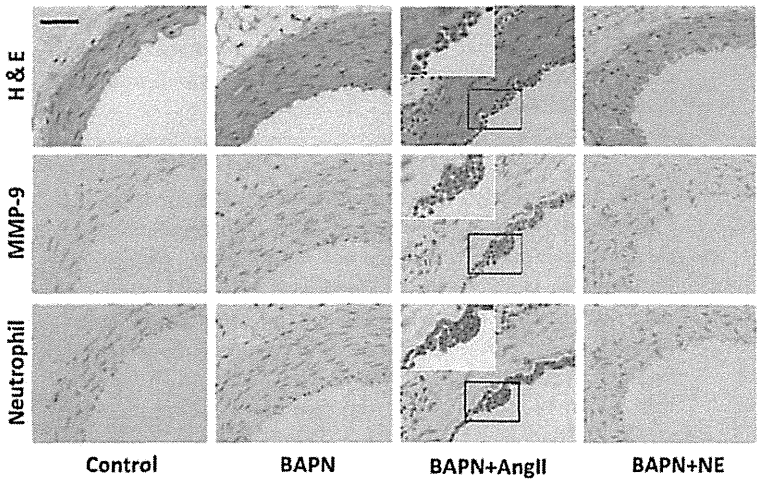

Figure 5. Infiltration of MMP9-positive neutrophils in the intima of nondissected lesions of BAPN/AngII-induced AAD thoracic aortas. MMP9 expression and neutrophil infiltration were examined by histology and immunohistochemistry in the aortas of untreated wild type mice (control) or wild type mice treated with BAPN alone, BAPN+AngII, and BAPN+NE. Note the accumulated MMP9-positive neutrophils in the intima of nondissected aorta from BAPN/AngII-treated mice. Inlets in the BAPN+AngII group show a higher-power view of the rectangular areas. Scale bar, 200 μm. MMP9 indicates matrix metalloproteinase 9; H&E, hematoxylin and eosin stain; BAPN, β-aminopropionitrile monofumarate; AngII, angiotensin II; AAD, acute aortic dissection; and NE, norepinephrine.

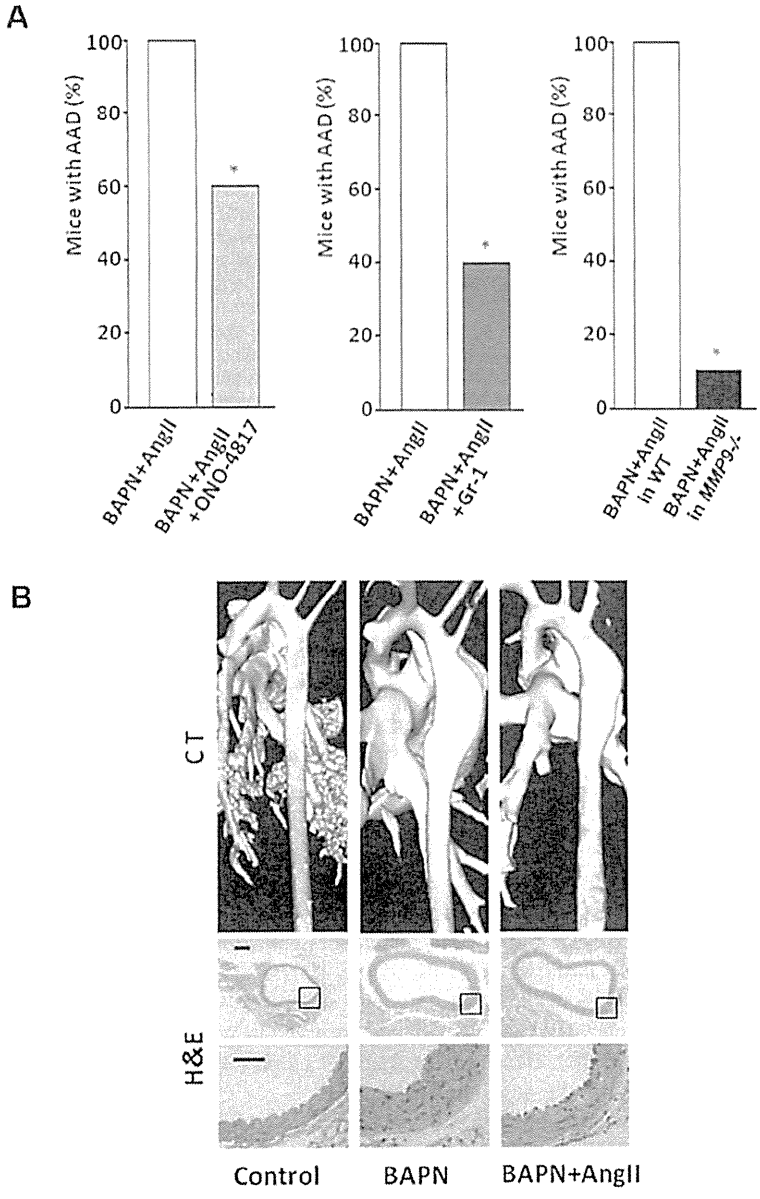

Figure 6. Pharmaceutical and genetic depletion of MMP9 or immunological depletion of neutrophils attenuates AAD incidence in mice. A, AAD incidence in BAPN/AngII-treated WT mice that were treated with ONO-4817 (BAPN+AngII+ONO-4817) (**left**) or anti-Gr-1 antibody (BAPN+AngII+Gr-1) (**middle**) and the incidence in BAPN/AngII-treated *MMP9*$^{-/-}$ mice (**right**) were compared with that in BAPN/AngII-treated WT mice (n=10 for each group). The probability value was adjusted with the Bonferroni method for pairwise comparisons. *$P<0.05$ versus BAPN/AngII-treated WT mice. B, Three-dimensional images of enhanced computed tomographic scan (**upper**) and histology (**middle** and **bottom**) of the aortas from *MMP9*$^{-/-}$ mice that were treated with vehicle for 4 weeks (control), BAPN alone for 4 weeks (BAPN), or BAPN for 4 weeks and then AngII for 24 hours (BAPN+AngII). Note that AAD formation is blocked in BAPN/AngII-treated *MMP9*$^{-/-}$ mice. (**Bottom**) High-power view of the rectangular areas in the middle panel. Scale bars, 200 μm and 100 μm for the middle and bottom panels, respectively. MMP9 indicates matrix metalloproteinase 9; AAD, acute aortic dissection; BAPN, β-aminopropionitrile monofumarate; AngII, angiotensin II; anti-Gr-1, anti-granulocyte-differentiation antigen-1; WT, wild type; and H&E, hematoxylin and eosin stain.

neutralizing antibody. The number of circulating neutrophils was reduced to 20% of control levels by intraperitoneal injection of the antibody for 48 hours prior to AngII infusion (data not shown), and, as expected, neutrophil depletion attenuated AAD incidence significantly (Figure 6A).

AngII-Induced Neutrophil Infiltration to Aortic Intima Independent From MMP9 Expression

Infiltration of neutrophils into the aortic intima was observed in BAPN/AngII-treated WT mice with or without ONO-4817 administration, as well as in BAPN/AngII-treated *MMP9*$^{-/-}$ mice (Figure 7A). Hence, these data demonstrate that AngII promotes neutrophil infiltration independent of MMP9 expression in our AAD model, but these results do not exclude the possibility that normal rates of neutrophil infiltration are maintained only within the noncross-linked, fragile vessel wall caused by chronic BAPN treatment. Thus, we further assessed the effect of AngII on neutrophil infiltration by infusing AngII in BAPN-untreated WT or *MMP9*$^{-/-}$ mice wherein vascular structural integrity is intact. As shown in Figure 7B, neutrophil infiltration into the aortic intima was unaffected between the 2 groups, indicating that AngII infusion evokes neutrophil infiltration to the intact aortic wall independent of MMP9 expression.

Discussion

In the current study, we demonstrated that serum levels of MMP9 and AngII are elevated in AAD patients, but not in patient populations with chronic, nonruptured aneurysms. Furthermore, increased circulating levels of MMP9 correlated with the presence of MMP9-positive neutrophils that accumulated in the aortic tissues of AAD patients. Given these findings from studies of human AAD specimens, we established a novel mouse model that develops AAD unfailingly within 24 hours of AngII infusion. This model was dependent on preconditioning mouse aortas with the lysyl oxidase

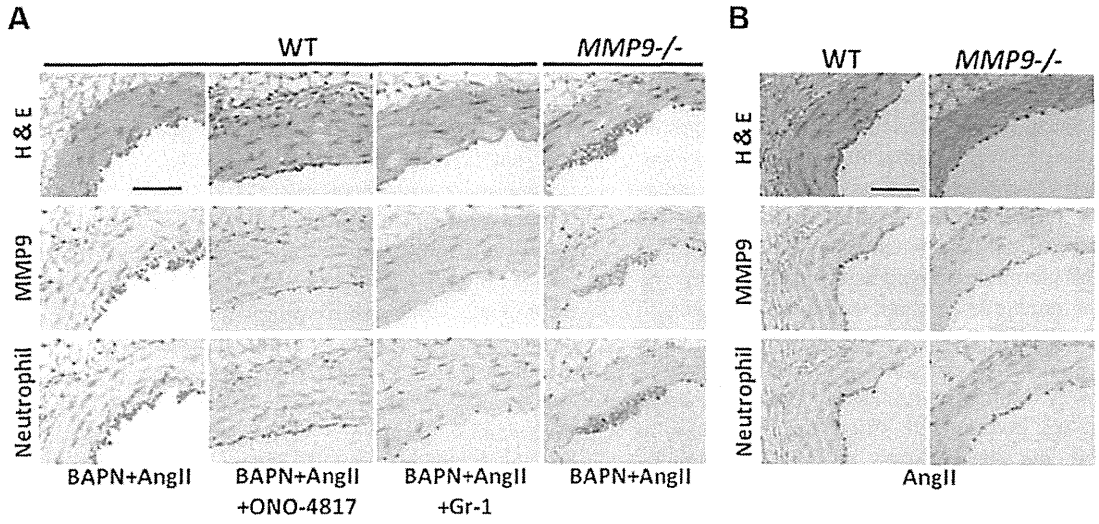

Figure 7. AngII-induced neutrophil infiltration in aortic intima is independent of MMP9 expression or BAPN treatment. A, Histological and immunohistochemical analyses of MMP9 expression and neutrophil infiltration in the aortic intima of the WT mice treated with BAPN and AngII (BAPN+AngII); BAPN, AngII, and ONO-4817 (BAPN+AngII+ONO-4817); or BAPN, AngII, and anti-Gr-1 antibody (BAPN+AngII+Gr-1); and those in the intima of the *MMP9*$^{-/-}$ mice treated with BAPN and AngII (BAPN+AngII) (n=10 for each group). Note that neutrophil infiltration is independent of MMP9 expression. Scale bar, 200 μm. B, Histological and immunohistochemical analyses of MMP9 expression and neutrophil infiltration in the aortic tissues of BAPN-untreated WT and *MMP9*$^{-/-}$ mice 24 hours after AngII infusion. Note that neutrophil infiltration is independent of BAPN treatment. Scale bar, 200 μm. AngII indicates angiotensin II; WT, wild type; MMP9, matrix metalloproteinase 9; H&E, hematoxylin and eosin stain; BAPN, β-aminopropionitrile monofumarate; and anti-Gr-1, anti-granulocyte-differentiation antigen-1.

inhibitor BAPN to create an aneurysmal, pre-AAD status in immature mice. Collagen and elastin cross-links, which are critical for maintaining vessel wall integrity, are disrupted by BAPN administration,[27] leading to the generation of mechanically fragile aortas that both display medial degeneration and develop aortic aneurysms. This type of aortic aneurysm is typically seen in human connective tissue diseases such as Marfan syndrome,[28] but the histology of cystic medial degeneration is commonly seen in aneurysms that arise secondary to aging and atherosclerosis as well.[3,4] It is not clearly elucidated whether aortic matrix cross-links are different between normal and aneurysmal aorta[29]; however, several studies from human pathological samples indicate that the composition of the aortic extracellular matrix changes as medial degeneration proceeds with enhanced deposition of proteoglycans and decreased collagen content, coupled with apoptosis of vascular smooth muscle cells.[30] These findings suggest that the aortic media and its matrix components are disorganized as a function of disease progression, thus leading to the generation of an aneurysmal aorta with weakened mechanical properties. As such, our mouse model would appear to recapitulate a similar state in which suitable triggers, such as AngII, precipitate the transition from a preconditioned, chronic aortic aneurysm to AAD.

Previous studies have suggested possible roles for MMP9 in the development of chronic atherosclerosis-derived aneurysms as well as connective tissue disease-related aortic aneurysm.[31–33] By contrast, our findings demonstrate that AAD formation itself proceeds in an MMP9-dependent fashion that is inhibited significantly by either pharmacological or genetic targeting of MMP9. A previous study by Gough et al[12] has shown that macrophages overexpressing autoactivating MMP9 induce atherosclerotic plaque rupture by disruptions of fibrous cap in apolipoprotein E mice, suggesting the ability of MMP9 to destroy aortic tissue. Altogether, these data support the notion that MMP9 is responsible for triggering aortic dissection from the preconditioned aneurysmal aorta. We have further demonstrated that neutrophil infiltration is observed in the intima of the predissecting aorta as well as in the dissected media, and that neutrophil depletion attenuates AAD incidence significantly. The importance of inflammation in the pathogenesis of vascular diseases is well documented, but until now, it has been difficult to determine whether neutrophil accumulation triggers dissection or occurs as a consequence of the massive vascular damage that develops during dissection. Because MMP9-positive neutrophils were confined to the intima of nondissected lesions while the dissected lesions displayed strong staining for MMP9-positive neutrophils primarily within the media, we posit that neutrophils infiltrate the intima at the initiation of dissection. Despite the importance of neutrophils, we cannot rule out the contribution of other immune effector cells that might be recruited subsequent to the inflammatory responses initiated by infiltrating neutrophils, as depleting neutrophils attenuated AAD, but not to the degree observed with *MMP9* targeting. Indeed, the upregulated *MMP9* mRNA levels detected in AAD aortic samples 24 hours after AngII infusion could result from nonneutrophil effector cells, because neutrophil MMP9 synthesis is mostly completed at earlier stages of differentiation, with mature neutrophils primarily storing MMP9 in granule compartments.[34] Nevertheless, the rapid induction of aortic dissection in our model as early as 6 hours after AngII infusion, in tandem with the accumulation of MMP9-positive neutrophils, supports the conclusion that infiltrating neutrophils trigger the initiation of dissection directly or indirectly.

MMP9 is a multifunctional proteinase endowed with the ability to degrade multiple extracellular matrix macromolecules, including types III, IV, and V collagens; denatured

collagens (ie, gelatin); and elastin.[11,35] Furthermore, MMP9 can modulate inflammatory responses by hydrolyzing a variety of cytokines and chemokines.[36] For example, MMP9 can activate prointerleukin-1,[37] increase the bioactivity of interleukin 8,[38] and promote interleukin 13-induced pulmonary inflammation,[39] while inactivating neutrophil chemokines such as growth-regulated oncogene and mature interleukin 1.[37,38] A recent clinical trial has shown that the treatment of aortic abdominal aneurysms with doxycycline, a nonspecific MMP inhibitor, reduced neutrophil and cytotoxic T-cell infiltration into the aneurysmal wall in association with decreased production of MMP9 and inflammatory cytokines.[40] MMP9 has also been reported to affect neutrophil chemotactic activity in lung injury models.[41,42] In the current study, however, we detected no differences in neutrophil infiltration within the aortic tissues of OND-4817-treated mice or between WT and *MMP9*$^{-/-}$ mice in our AAD model. Furthermore, in contrast to malignant cells, with MMP-dependent invasive activity that is affected by collagen cross-links,[43] our study showed that neutrophils infiltrate aortic tissues similarly in both BAPN-treated and -untreated mice. Together, these data suggest that neutrophil infiltration proceeds independently of MMP9 activity or collagen cross-links in this model system.

A detailed mechanism regarding how MMP9 contributes to the initiation of AAD remains to be defined. In recent studies using *Fibrillin1*$^{-/-}$ mice, which develop AAD spontaneously secondary to connective tissue defect, the elevation of transforming growth factor levels and its downstream signaling cascade contribute to the pathogenesis of aortic aneurysm and dissection.[44] In this model, MMP2 and MMP9 were both upregulated, and doxycycline attenuated disease progression.[31,32] Because MMP9 is a potent activator of latent transforming growth factor ,[45] it is interesting to speculate that upregulated MMP9 activity may trigger AAD by in situ activation of transforming growth factor in the affected aortic media of the mice.

Last, our study has validated AngII as a potent inducer of mouse AAD, a result that complements the higher levels of AngII detected in our AAD patient population. Long-term AngII infusion is known to lead to spontaneous aortic dissection in atherosclerosis models using *apoE*$^{-/-}$ mice.[46] Recent studies have also demonstrated that Losartan, an antagonist of the AngII receptor, AT1, prevents aortic aneurysm development and aortic root dilation in Marfanoid mice and humans.[44,47] It is clear that the role of AngII in the induction of AAD is not a result of vasopressor effects alone, because NE failed to trigger AAD in our model despite similar levels of hypertension. One of the significant differences between the aortic lesions observed in BAPN/AngII-treated versus BAPN/NE-treated WT mice was the presence of neutrophil infiltrates in the BAPN/AngII-treated mice, suggesting that AngII acts as a potent stimulus for neutrophil infiltration into the aorta intima. Indeed, recent studies indicate that AngII can induce neutrophil infiltration.[22,23] In addition, AngII is also able to activate neutrophils and stimulate the nicotinamide adenine dinucleotide phosphate (NADPH) oxidase-dependent production of reactive oxygen metabolites, which may promote the oxidative autoactivation of pro-MMP9.[48,49] In the current study, we could show the gelatinolytic metalloproteinase activity and superoxide production in the neutrophil-infiltrated dissecting aortic tissue from the BAPN/AngII-treated mice. Thus, AngII likely plays a key role in triggering AAD onset not only by attracting neutrophils to the affected sites, but also by stimulating the release and activation of pro-MMP9.

This study has a few limitations. First, we used a mouse model to demonstrate the role of neutrophil-derived MMP9 activity in AAD formation. Because mouse models do not recapitulate human disease progression stringently, the results of our AAD model may be different in humans. In the mouse model, AAD was induced in the descending thoracic aorta by AngII infusion to the young mice treated with BAPN. Preconditioning for the AAD induction (ie, aneurism formation) by BAPN treatment is artificial and may be applicable for AAD in patients with connective tissue disorders but not for commonly observed AAD in humans, such as our patients in the current study. Another limitation of this study is that the activation mechanism of pro-MMP9 within aortic tissues has not been examined in mouse or human AAD. Although our study on the mouse model has suggested possible involvement of reactive oxygen species in the activation, detailed studies regarding whether pro-MMP9 activation and AAD incidence are suppressed by antioxidant therapy, and which reactive oxygen species are required for pro-MMP9 activation in coculture system of neutrophils and smooth muscle cells, will be necessary. Moreover, reactive oxygen species-mediated pro-MMP9 activation in human aortic tissues from AAD patients needs to be investigated by future work.

AAD is a potentially fatal disease, the prompt diagnosis and treatment of which are required for successful intervention. Although the fibrin product, D-dimer, is the only established biomarker for AAD, the differential diagnosis of AMI versus pulmonary embolism, which displays similar symptoms to that of AAD, can be difficult.[50,51] In this context, MMP9 could serve as a potential biomarker for the diagnosis of AAD. Furthermore, although the dominant treatment for AAD relies on surgical reinforcement of the affected aorta, our data raise the possibility that the preventive administration of AngII receptor blockers or MMP9-specific inhibitors to patients at risk with nonruptured atherosclerotic aneurysm could prove useful as effective therapeutics to reduce AAD incidence.

Sources of Funding

This work was supported by Grant-in-Aid from the Ministry of Education, Science and Culture of Japan (Dr Kurihara and Dr Shimizu-Hirota), and Grant-in-Aid from the Ministry of Education, Science and Culture of Japan and the grant from the Ministry of Health, Labor and Welfare (Research Group of Intractable Vasculitis) Japan (Dr Okada).

Disclosures

None.

References

1. Golledge J, Eagle KA. Acute aortic dissection. *Lancet*. 2008;372:55–66.
2. Pretre R, Von Segesser LK. Aortic dissection. *Lancet*. 1997;349:1461–1464.

3. Schlatmann TJ, Becker AE. Histologic changes in the normal aging aorta: implications for dissecting aortic aneurysm. *Am J Cardiol.* 1977;39: 13–20.
4. Carlson RG, Lillehei CW, Edwards JE. Cystic medial necrosis of the ascending aorta in relation to age and hypertension. *Am J Cardiol.* 1970;25:411–415.
5. Eldadah ZA, Brenn T, Furthmayr H, Dietz HC. Expression of a mutant human fibrillin allele upon a normal human or murine genetic background recapitulates a Marfan cellular phenotype. *J Clin Invest.* 1995;95: 874–880.
6. Maki JM, Rasanen J, Tikkanen H, Sormunen R, Makikallio K, Kivirikko KI, Soininen R. Inactivation of the lysyl oxidase gene *Lox* leads to aortic aneurysms, cardiovascular dysfunction, and perinatal death in mice. *Circulation.* 2002;106:2503–2509.
7. Kumar D, Trent MB, Boor PJ. Allylamine and beta-aminopropionitrile induced aortic medial necrosis: mechanisms of synergism. *Toxicology.* 1998;125:107–115.
8. Page RC, Benditt EP. Molecular diseases of connective and vascular tissues: 3. The aldehyde content of normal and lathyritic soluble collagen. *Lab Invest.* 1968;18:124–130.
9. Galis ZS, Sukhova GK, Lark MW, Libby P. Increased expression of matrix metalloproteinases and matrix degrading activity in vulnerable regions of human atherosclerotic plaques. *J Clin Invest.* 1994;94: 2493–2503.
10. Newby AC. Metalloproteinases and vulnerable atherosclerotic plaques. *Trends Cardiovasc Med.* 2007;17:253–258.
11. Katsuda S, Okada Y, Imai K, Nakanishi I. Matrix metalloproteinase-9 (92-kd gelatinase/type IV collagenase equals gelatinase B) can degrade arterial elastin. *Am J Pathol.* 1994;145:1208–1218.
12. Gough PJ, Gomez IG, Wille PT, Raines EW. Macrophage expression of active MMP-9 induces acute plaque disruption in apoE-deficient mice. *J Clin Invest.* 2006;116:59–69.
13. Loftus IM, Naylor AR, Goodall S, Crowther M, Jones L, Bell PR, Thompson MM. Increased matrix metalloproteinase-9 activity in unstable carotid plaques: a potential role in acute plaque disruption. *Stroke.* 2000; 31:40–47.
14. Wilson WR, Anderton M, Schwalbe EC, Jones JL, Furness PN, Bell PR, Thompson MM. Matrix metalloproteinase-8 and -9 are increased at the site of abdominal aortic aneurysm rupture. *Circulation.* 2006;113: 438–445.
15. Nagashima H, Uto K, Sakomura Y, Aoka Y, Sakuta A, Aomi S, Hagiwara N, Kawana M, Kasanuki H. An angiotensin-converting enzyme inhibitor, not an angiotensin II type-1 receptor blocker, prevents beta-aminopropionitrile monofumarate-induced aortic dissection in rats. *J Vasc Surg.* 2002;36: 818–823.
16. Shimizu-Hirota R, Sasamura H, Kuroda M, Kobayashi E, Hayashi M, Saruta T. Extracellular matrix glycoprotein biglycan enhances vascular smooth muscle cell proliferation and migration. *Circ Res.* 2004;94: 1067–1074.
17. Hariya A, Takazawa K, Yamamoto T, Amano A. ONO-4817, a novel matrix metalloproteinase inhibitor, attenuates allograft vasculopathy in a rat cardiac transplant. *J Heart Lung Transplant.* 2004;23: 1163–1169.
18. Shirahane K, Yamaguchi K, Koga K, Watanabe M, Kuroki S, Tanaka M. Hepatic ischemia/reperfusion injury is prevented by a novel matrix metalloproteinase inhibitor, ONO-4817. *Surgery.* 2006;139:653–664.
19. Yamada A, Uegaki A, Nakamura T, Ogawa K. ONO-4817, an orally active matrix metalloproteinase inhibitor, prevents lipopolysaccharide-induced proteoglycan release from the joint cartilage in guinea pigs. *Inflamm Res.* 2000;49:144–146.
20. Nozawa H, Chiu C, Hanahan D. Infiltrating neutrophils mediate the initial angiogenic switch in a mouse model of multistage carcinogenesis. *Proc Natl Acad Sci U S A.* 2006;103:12493–12498.
21. Daugherty A, Manning MW, Cassis LA. Angiotensin II promotes atherosclerotic lesions and aneurysms in apolipoprotein E-deficient mice. *J Clin Invest.* 2000;105:1605–1612.
22. Abu Nabah YN, Losada M, Estelles R, Mateo T, Company C, Piqueras L, Lopez-Gines C, Sarau H, Cortijo J, Morcillo EJ, Jose PJ, Sanz MJ. CXCR2 blockade impairs angiotensin II-induced CC chemokine synthesis and mononuclear leukocyte infiltration. *Arterioscler Thromb Vasc Biol.* 2007;27:2370–2376.
23. Arndt PG, Young SK, Poch KR, Nick JA, Falk S, Schrier RW, Worthen GS. Systemic inhibition of the angiotensin-converting enzyme limits lipopolysaccharide-induced lung neutrophil recruitment through both bradykinin and angiotensin II-regulated pathways. *J Immunol.* 2006;177: 7233–7241.
24. Guo RW, Yang LX, Wang H, Liu B, Wang L. Angiotensin II induces matrix metalloproteinase-9 expression via a nuclear factor-kappaB-dependent pathway in vascular smooth muscle cells. *Regul Pept.* 2008; 147:37–44.
25. Szocs K, Lassegue B, Sorescu D, Hilenski LL, Valppu L, Couse TL, Wilcox JN, Quinn MT, Lambeth JD, Griendling KK. Upregulation of Nox-based NAD(P)H oxidases in restenosis after carotid injury. *Arterioscler Thromb Vasc Biol.* 2002;22:21–27.
26. Mauro A, Buscemi M, Gerbino A. Immunohistochemical and transcriptional expression of matrix metalloproteinases in full-term human umbilical cord and human umbilical vein endothelial cells. *J Mol Histol.* 2010;41:367–377.
27. Bruel A, Ortoft G, Oxlund H. Inhibition of cross-links in collagen is associated with reduced stiffness of the aorta in young rats. *Atherosclerosis.* 1998;140:135–145.
28. Schlatmann TJ, Becker AE. Pathogenesis of dissecting aneurysm of aorta: comparative histopathologic study of significance of medial changes. *Am J Cardiol.* 1977;39:21–26.
29. Gaetani P, Tartara F, Grazioli V, Tancioni F, Infuso L, Rodriguez y Baena R. Collagen cross-linkage, elastolytic and collagenolytic activities in cerebral aneurysms: a preliminary investigation. *Life Sci.* 1998;63: 285–292.
30. Tang PC, Coady MA, Lovoulos C, Dardik A, Aslan M, Elefteriades JA, Tellides G. Hyperplastic cellular remodeling of the media in ascending thoracic aortic aneurysms. *Circulation.* 2005;112:1098–1105.
31. Chung AW, Au Yeung K, Sandor GG, Judge DP, Dietz HC, van Breemen C. Loss of elastic fiber integrity and reduction of vascular smooth muscle contraction resulting from the upregulated activities of matrix metalloproteinase-2 and -9 in the thoracic aortic aneurysm in Marfan syndrome. *Circ Res.* 2007;101:512–522.
32. Chung AW, Yang HH, Radomski MW, van Breemen C. Long-term doxycycline is more effective than atenolol to prevent thoracic aortic aneurysm in Marfan syndrome through the inhibition of matrix metalloproteinase-2 and -9. *Circ Res.* 2008;102:e73–e85.
33. McMillan WD, Pearce WH. Increased plasma levels of metalloproteinase-9 are associated with abdominal aortic aneurysms. *J Vasc Surg.* 1999;29: 122–127; discussion 127–129.
34. Borregaard N, Sehested M, Nielsen BS, Sengelov H, Kjeldsen L. Biosynthesis of granule proteins in normal human bone marrow cells: gelatinase is a marker of terminal neutrophil differentiation. *Blood.* 1995;85: 812–817.
35. Okada Y, Gonoji Y, Naka K, Tomita K, Nakanishi I, Iwata K, Yamashita K, Hayakawa T. Matrix metalloproteinase 9 (92-kDa gelatinase/type IV collagenase) from HT 1080 human fibrosarcoma cells: purification and activation of the precursor and enzymic properties. *J Biol Chem.* 1992; 267:21712–21719.
36. Parks WC, Wilson CL, Lopez-Boado YS. Matrix metalloproteinases as modulators of inflammation and innate immunity. *Nat Rev Immunol.* 2004;4:617–629.
37. Schonbeck U, Mach F, Libby P. Generation of biologically active IL-1 beta by matrix metalloproteinases: a novel caspase-1-independent pathway of IL-1 beta processing. *J Immunol.* 1998;161:3340–3346.
38. Van den Steen PE, Proost P, Wuyts A, Van Damme J, Opdenakker G. Neutrophil gelatinase B potentiates interleukin-8 tenfold by aminoterminal processing, whereas it degrades CTAP-III, PF-4, and GRO-alpha and leaves RANTES and MCP-2 intact. *Blood.* 2000;96: 2673–2681.
39. Lanone S, Zheng T, Zhu Z, Liu W, Lee CG, Ma B, Chen Q, Homer RJ, Wang J, Rabach LA, Rabach ME, Shipley JM, Shapiro SD, Senior RM, Elias JA. Overlapping and enzyme-specific contributions of matrix metalloproteinases-9 and -12 in IL-13-induced inflammation and remodeling. *J Clin Invest.* 2002;110:463–474.
40. Lindeman JH, Abdul-Hussien H, van Bockel JH, Wolterbeek R, Kleemann R. Clinical trial of doxycycline for matrix metalloproteinase-9 inhibition in patients with an abdominal aneurysm: doxycycline selectively depletes aortic wall neutrophils and cytotoxic T cells. *Circulation.* 2009;119:2209–2216.
41. Albaiceta GM, Gutierrez-Fernandez A, Parra D, Astudillo A, Garcia-Prieto E, Taboada F, Fueyo A. Lack of matrix metalloproteinase-9 worsens ventilator-induced lung injury. *Am J Physiol Lung Cell Mol Physiol.* 2008;294:L535–L543.
42. Keck T, Balcom JH, Fernandez-del Castillo C, Antoniu BA, Warshaw AL. Matrix metalloproteinase-9 promotes neutrophil migration and

alveolar capillary leakage in pancreatitis-associated lung injury in the rat. *Gastroenterology*. 2002;122:188–201.
43. Sabeh F, Shimizu-Hirota R, Weiss SJ. Protease-dependent versus -independent cancer cell invasion programs: three-dimensional amoeboid movement revisited. *J Cell Biol*. 2009;185:11–19.
44. Habashi JP, Judge DP, Holm TM, Cohn RD, Loeys BL, Cooper TK, Myers L, Klein EC, Liu G, Calvi C, Podowski M, Neptune ER, Halushka MK, Bedja D, Gabrielson K, Rifkin DB, Carta L, Ramirez F, Huso DL, Dietz HC. Losartan, an AT1 antagonist, prevents aortic aneurysm in a mouse model of Marfan syndrome. *Science*. 2006;312:117–121.
45. Yu Q, Stamenkovic I. Cell surface-localized matrix metalloproteinase-9 proteolytically activates TGF-beta and promotes tumor invasion and angiogenesis. *Genes Dev*. 2000;14:163–176.
46. Saraff K, Babamusta F, Cassis LA, Daugherty A. Aortic dissection precedes formation of aneurysms and atherosclerosis in angiotensin II-infused, apolipoprotein E-deficient mice. *Arterioscler Thromb Vasc Biol*. 2003;23:1621–1626.
47. Brooke BS, Habashi JP, Judge DP, Patel N, Loeys B, Dietz HC, III. Angiotensin II blockade and aortic-root dilation in Marfan's syndrome. *N Engl J Med*. 2008;358:2787–2795.
48. El Bekay R, Alvarez M, Monteseirin J, Alba G, Chacon P, Vega A, Martin-Nieto J, Jimenez J, Pintado E, Bedoya FJ, Sobrino F. Oxidative stress is a critical mediator of the angiotensin II signal in human neutrophils: involvement of mitogen-activated protein kinase, calcineurin, and the transcription factor NF-kappaB. *Blood*. 2003;102:662–671.
49. Weiss SJ, Peppin G, Ortiz X, Ragsdale C, Test ST. Oxidative autoactivation of latent collagenase by human neutrophils. *Science*. 1985;227:747–749.
50. Eggebrecht H, Naber CK, Bruch C, Kroger K, von Birgelen C, Schmermund A, Wichert M, Bartel T, Mann K, Erbel R. Value of plasma fibrin D-dimers for detection of acute aortic dissection. *J Am Coll Cardiol*. 2004;44:804–809.
51. Weber T, Hogler S, Auer J, Berent R, Lassnig E, Kvas E, Eber B. D-dimer in acute aortic dissection. *Chest*. 2003;123:1375–1378.

CLINICAL PERSPECTIVE

Acute aortic dissection (AAD) is a potentially fatal vascular disease, and prompt diagnosis and treatment by timely surgery are required for survival of the patients. No efficient biomarkers are available for diagnosis of AAD prior to determination of the disease by computed tomography. Medial degeneration is known as an important risk factor for the development of AAD; however, the emergent nature of the disease and the paucity of animal models prevent us from studying the molecular mechanisms for triggering the disease. We found that matrix metalloproteinase 9 (MMP9) and angiotensin II were increased significantly in blood samples from AAD patients compared with those from normal subjects and the patients with nonruptured aortic aneurysm. This was accompanied by enhanced infiltrations of MMP9-producing neutrophils in the dissected aortas. Based on the data, we established a mouse model of AAD, which was induced by infusion of angiotensin II to mice pretreated with β-aminopropionitrile monofumarate (a lysyl oxidase inhibitor). All mice exhibited AAD within 24 hours after angiotensin II infusion. Aortic tissue from the AAD mice showed enhanced expression and activity of MMP9, and MMP9-immunoreactive neutrophils were infiltrated in both dissected media and intima of nondissected lesions. Genetic depletion or pharmaceutical inhibition of MMP9 and neutrophil ablation attenuated the AAD incidence. These data demonstrate that neutrophil-derived MMP9 is responsible for triggering AAD in this model. Taken together, MMP9 could serve as a potential biomarker for diagnostic screening of AAD, and administration of angiotensin II receptor blockers or MMP9 inhibitors could be effective therapeutic approaches to AAD.

J Artif Organs
DOI 10.1007/s10047-013-0694-4

ORIGINAL ARTICLE

Numerical analysis of blood flow distribution in 4- and 3-branch vascular grafts

Chikako Konoura · Takanobu Yagi · Masanori Nakamura · Kiyotaka Iwasaki · Yi Qian · Shigeo Okuda · Akihiro Yoshitake · Hideyuki Shimizu · Ryohei Yozu · Mitsuo Umezu

Received: 11 December 2012 / Accepted: 30 January 2013

Abstract Trifurcated arch grafts (3-branch grafts) are now being used to repair the thoracic aorta in addition to conventional arch grafts (4-branch grafts). The anatomical shape of the 3-branch graft is different from the original vessel, so it is necessary for clinical application to evaluate blood flow distribution in the graft to assess whether there is adequate blood flow to the target organs. To achieve this, we developed a computational fluid dynamics (CFD) method to evaluate blood flow distribution in the grafts. Aortic blood flow was measured by phase-contrast magnetic resonance imaging (PC-MRI), and flow distribution into the branched vessels was obtained. The MRI image was used to create a patient-specific image model that represents the geometry of the aortic arch. The CFD analysis method was employed to determine a boundary condition of the blood flow analysis in the aorta using a patient-specific image model. We also created simplified models of 4-branch and 3-branch grafts and used our CFD analysis method to compare blood flow distribution among simplified models. It was found that blood flow distribution in the descending aorta was 71.3 % for the 4-branch graft and 67.7 % for the 3-branch graft, indicating that a sum of branching flow in the 3-branch graft was almost the same as the one in the 4-branch graft. Therefore, there is no major concern about implanting a new 3-branch graft. Our CFD analysis method may be applied to estimate blood flow distribution of a newly developed vascular graft prior to its clinical use and provide useful information for safe use of the graft.

Keywords Arch graft · Blood flow distribution · CFD · PC-MRI

C. Konoura · K. Iwasaki · M. Umezu (✉)
TWIns (Tokyo Women's Medical University-Waseda University Joint Institution) for Advanced Biomedical Sciences,
2-2 #03C204 Wakamatsucho, Shinjuku, Tokyo 162-8480, Japan
e-mail: umezu@waseda.jp

C. Konoura (✉)
School of Health Sciences, Tokyo University of Technology,
5-23-22 Nishi-Kamata, Ohta, Tokyo 144-8535, Japan
e-mail: konoura@stf.teu.ac.jp

T. Yagi · K. Iwasaki · M. Umezu
Faculty of Science and Engineering, Waseda University,
Tokyo, Japan

T. Yagi · M. Nakamura · K. Iwasaki · Y. Qian · M. Umezu
Research Institute for Science and Engineering,
Waseda University, Tokyo, Japan

M. Nakamura
Saitama University Graduate School of Science and Engineering, Saitama, Japan

Y. Qian
Australian School of Advanced Medicine,
Macquarie University, Macquarie Park, Australia

S. Okuda
Division of Diagnostic Radiology,
Department of Radiology, Keio University School of Medicine,
Tokyo, Japan

A. Yoshitake · H. Shimizu · R. Yozu
Division of Cardiovascular Surgery,
Department of Surgery, Keio University School of Medicine,
Tokyo, Japan

Published online: 24 February 2013

Introduction

Arch grafts (4-branch grafts) with the same shape as the aortic arch are conventionally used to repair the large thoracic vessel. Trifurcated arch grafts (3-branch grafts) are now also being used to detain a stent in the aortic arch where the brachiocephalic artery (BA), left common carotid artery (LCCA), and left subclavian artery (LSCA) branch off. Stent detention possibly causes abnormal blood flow distribution into these vessels [1–7]. Clinicians need to know whether adequate blood flow is delivered into each branched vessel because the 3-branch graft replacement makes the shape of the aortic arch geometrically different from the shape when using a 4-branch graft replacement (Fig. 1).

Evaluating blood flow distribution in 3-branch grafts by computational fluid dynamics (CFD) has not been performed at preclinical trial. Because measurements of pressure and blood flow are not easy tasks in clinical practice, and hemodynamic pressure difference and blood flow within the branch are not known quantitatively, it is difficult to estimate blood flow distribution after an artificial blood vessel is implanted, particularly when the artificial blood vessel has a different geometry from the natural one. The purpose of this study was to investigate blood flow distribution of each aortic-branch blood vessel and establish a method using CFD to compare that distribution. Furthermore, a comparison of blood flow distribution between the 4- and 3-branch grafts was performed to provide useful information for safe surgery.

Methods

Blood flow measurement by PC-MRI

Blood flow in the aorta of three healthy individuals was measured by phase-contrast magnetic resonance imaging (PC-MRI, HDMR Signa EXCITE HD1.5T, GE Healthcare, Waukesha, WI, USA) to estimate blood flow distribution. All individuals enrolled in this research gave their informed consent, and the study protocol was approved by our institutional committee on human research. PC-MRI was acquired with electrocardiographic (ECG) synchronization under the following conditions: 2.9-ms repetition time (TR), 250 cm/s velocity encoding, 20° flip angle (FA), 10-mm thickness, 256 × 256 matrix, and 32 × 24-cm field of view (FOV). We measured blood flow in five arteries: ascending aorta (AAo), descending aorta (DAo), BA, LCCA, and LSCA. Blood flow was measured cross-sectionally three to five times for the AAo and DAo and three times for the BA, LCCA, and LSCA. Intensity-image data were processed through an edge filter (Matlab R2012a Ver. 7.14.0.739, MathWorks, Natick, MA, USA) and digitized. This enabled us to measure blood flow and calculate blood flow distribution (Fig. 2). Total volume of blood flow in each branch over one cardiac cycle was calculated by summing the blood flow measured at each instance multiplied by a time interval between measurements. Total outlet blood flow (sum of the flows of DAo, BA, LCCA, and LSCA) was 10 % higher than the inlet flow (AAo) [8, 9]. We considered that the difference was caused by slightly incorrect detection of the vessel wall, so we calculated blood flow distributions with their values normalized by the ratio of the outlet flow to the inlet flow [8].

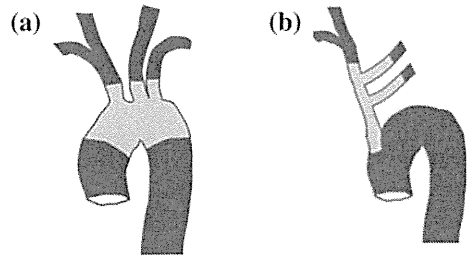

Fig. 1 Shape of the aortic arch after a graft transplant (*gray*). **a** Four-branch graft, **b** 3-branch graft

CFD analysis based on blood flow distribution into descending aorta

CFD models

1. Individual-specific model

Individual-specific model was created from MRI images of the aorta. The aortic arch image was extracted as a semicircular arc (Fig. 3a). BA, LCCA, and LSCA lengths were assumed to be approximately 40 mm.

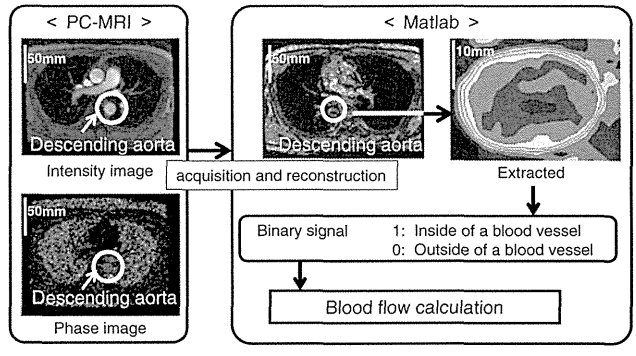

Fig. 2 Blood flow measurement by phase-contrast magnetic resonance imaging (PC-MRI). The image of the target blood vessel (DAo) is extracted from the intensity image. The phase image (DAo) is from processing software Matlab. Blood flow is calculated from the intravascular phase signal

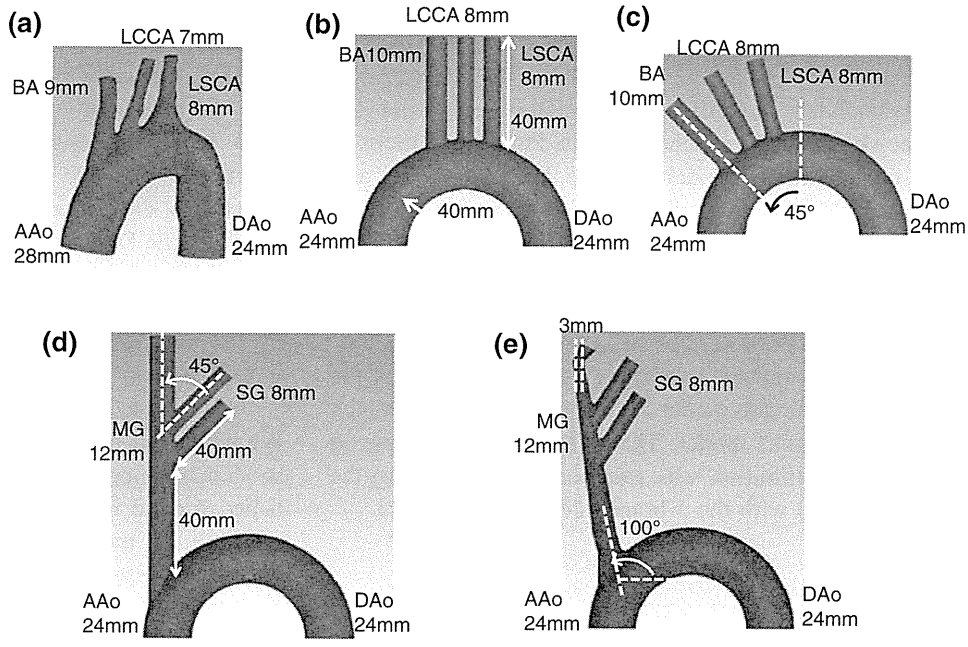

Fig. 3 Individual-specific and simplified computational fluid dynamics (CFD) models. **a** Individual-specific, **b** 4-branch benchmark, **c** 4-branch aslope, **d** 3-branch model, and **e** 3-branch deformation. *AAO* ascending aorta, *DAO* descending aorta, *BA* brachiocephalic artery, *LCCA* left common carotid artery, *LSCA* left subclavian artery, *MG* main graft, *SG* side graft

2. Simplified models

We created four simplified models (Fig. 3b–e), based on an individual-specific model (Fig. 3a):

(a) Four-branch benchmark model
(b) Four-branch aslope model
(c) Three-branch model
(d) Three-branch deformation model.

Deformation is generally called "kink" status. The 4-branch benchmark model has three branches that stem from the top of the arch, and the 4-branch aslope model has three branches placed at a 45° angle inclination to the AAo. The aslope model was considered to represent the expected geometry of the graft after the replacement operation. The 3-branch model has a main graft (MG) at right angles to the inlet of an AAo. The 3-branch deformation model has a MG, which is kinked at the BA site. In addition, because the geometry of the artery of the patient with an aortic aneurysm after an operation became normal, we assumed the form of the normal blood vessel. Diameters of these vessels were assumed to be the same as commercialized grafts. Diameters of arteries of the 4-branch graft model are AAo and DAo, 24 mm; BA, 10 mm; LCCA, 8 mm; and LSCA, 8 mm. The 3-branch graft model has a 12-mm-diameter MG and two 8-mm-diameter side grafts. In the 3-branch deformation model, a kink was made in the vicinity of anastomosis between BA and MG by narrowing a diameter from 12 to 3 mm. The diameter of the arc of the aortic arch is 80 mm for both the 4- and 3-branch grafts. CFD analysis was performed using ANSYS (Ver. 13.0, ANSYS, Inc., Canonsburg, PA, USA).

CFD analysis conditions

Cardiac output, the inlet boundary condition, was set as a normal 5.0 l/min [10]. Although analysis usually assumes that all outlet boundary conditions are the same, this assumption cannot apply to our method because it does not match the blood flow distribution obtained from PC-MRI. An outlet pressure difference means the difference in peripheral resistance. Blood flow distribution was calculated under the condition of 0 mmHg at the outlet pressure of the three branches (BA, LCCA, LSCA). On the other hand, DAo pressure was adjusted by a procedure in order to match the blood flow distribution obtained from CFD with that obtained from PC-MRI. The same method was applied to determine outlet boundary conditions of the 4-branch model. Blood flow distribution in 3-branch models was obtained with the same boundary conditions as for 4-branch models.

Intravascular mesh generation was achieved with prism/tetra mesh with 5-grid layers placed near the wall to assure a boundary layer [11]. Although it was known that the accuracy of CFD results relies on mesh quality and boundary conditions, our mesh generation method has already been verified and mesh quality secured [11]. The number of elements in the 4-branch aslope model was 983,117. The error of the 4-branch aslope model was 0.9 %. Mesh independence was confirmed in the 4-branch aslope model by using finer meshes. We performed analysis assuming a blood density of 1,060 kg/m^3, viscosity coefficient of 0.004 Pa s, rigid wall model, and steady and laminar flow [10–12].

Examination of blood flow distributions in the 4- and 3-branch models

Outlet boundary conditions were determined from the 4-branch benchmark model. We applied these conditions to the 4-branch aslope model and the 3-branch model and compared blood flow distribution of each model.

Examination of blood flow distributions in the 3-branch model and 3-branch deformation model

The outlet boundary condition determined from the 4-branch benchmark model was applied to the 3-branch deformation (kink) model. The effect of deformation on blood flow distribution was examined by comparing the 3-branch model with the 3-branch deformation model.

Results

Blood flow measurement by PC-MRI

Table 1 shows the blood flow distribution of healthy individuals. Cases 1–3 represent our measurements, and cases 4–6 are from a previously published article [8].

Blood flow distributions were 66.0–76.9 % for the DAo, 10.8–14.6 % for the right-side artery (BA) and 11.3–19.3 % for the left-side arteries (LCCA and LSCA). Distribution ratio of right to left was from 1:1 to 1:1.4. Welch's *t* test indicated that there was no statistically significant difference in blood flow data between right and left side.

Examination of outlet boundary conditions

Individual-specific model

A individual-specific model was created based on case 1 in Table 1. The result is shown in Fig. 4. Blood flow distribution in the DAo was 86.4 % when there was no pressure difference between the outlet of DAo and the outlet of the three-branch site of the aortic arch. It agreed with the blood flow distribution in DAo by PC-MRI and CFD when the outlet pressure difference was set at 0.9 mmHg (Fig. 4). This method enabled us to obtain a blood flow distribution that corresponded with the distribution in the DAo, which we obtained from PC-MRI. We used this method to perform CFD analysis to estimate blood flow distribution in other models.

4-Branch benchmark model

We examined outlet boundary conditions of the 4-branch benchmark model using the CFD analysis method established for the individual-specific model. Blood flow distribution in the DAo was 80.6 % when the pressure difference between the DAo outlet the outlet of the three-branch site of the aortic arch was 0.0 mmHg, and 71.3 % when the outlet pressure difference was 0.4 mmHg. It agreed with the blood flow distribution in the DAo by PC-MRI and CFD (Fig. 5). We set an outlet pressure difference of 0.4 mmHg as the outlet boundary condition of the benchmark model.

Blood flow distribution in 4-branch aslope model and 3-branch model

Outlet boundary conditions that we determined for the 4-branch benchmark model (pressure difference of 0.4 mmHg) were applied to the 4-branch aslope model and 3-branch model to obtain blood flow distribution. Results are shown in Table 2. Blood flow distribution in the DAo was 71.1 % for the 4-branch aslope model and 67.7 % for the 3-branch model. In both cases, the obtained values fell inside the variance range of blood flow distribution in the DAo of healthy individuals (Table 1). In the 3-branch model, the distribution ratio of right to left was 1:0.5 (Table 2).

Table 1 Blood flow distribution of healthy individuals (%)

Case no.	Sex	Age	Height (m)	Weight (kg)	Descending aorta	Right (BA)	Left (LCCA, LSCA)	References
1	Male	34	1.78	80	69.9	13.7	16.2	–
2	Male	39	1.67	78	76.8	10.8	12.3	–
3	Male	38	1.75	74	76.9	11.7	11.3	–
4	Male	25	1.69	62	68.0	14.6	17.3	[7]
5	Male	22	1.75	56	66.0	14.4	19.3	[7]
6	Male	47	1.67	64	69.1	13.0	17.8	[7]
Average ± SD	–	34 ± 9	1.72 ± 0.05	69 ± 10	71.1 ± 4.6	13.0 ± 1.5	15.7 ± 3.2	

SD standard deviation, *BA* brachiocephalic artery, *LCCA* left common carotid artery, *LSCA* left subclavian artery

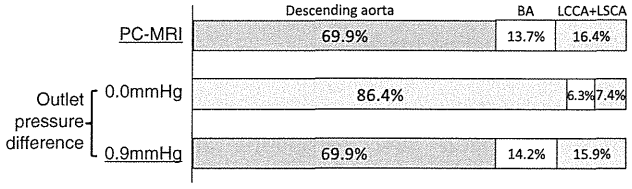

Fig. 4 Blood flow distribution by outlet pressure difference in the individual-specific image model (case 1). *BA* brachiocephalic artery, *LCCA* left common carotid artery, *LSCA* left subclavian artery

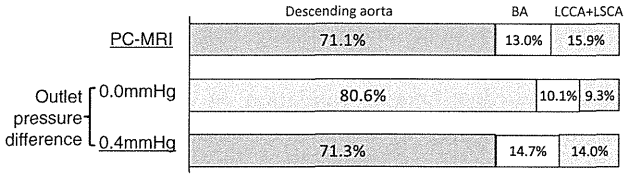

Fig. 5 Blood flow distribution with upper outlet pressure difference of the descending aorta of the benchmark model. *BA* brachiocephalic artery, *LCCA* left common carotid artery, *LSCA* left subclavian artery

Blood flow distribution in 3-branch model and 3-branch deformation model

Blood flow distribution of the DAo with the 3-branch deformation model was 77.6 % (Table 2). As shown in Table 1, the maximum blood flow distribution of the DAo in healthy individuals was 76.9 %, and the value of the deformation mode (77.6 %) exhibited slightly higher flow than the maximum limit of healthy individuals. On the other hand, blood flow distribution of the BA in the 4-branch benchmark model, 4-branch aslope model, and 3-branch model was 14.7 %, 13.9 %, and 21.2 %, respectively. However, blood flow distribution of the BA with the 3-branch deformation model was only 8.6 %. Although there was not a large difference in blood flow distribution of the DAo between normal and deformation models, distribution in the BA indicated a large difference. Therefore, in the practical clinical usage, it is important to avoid a kink status as much as possible.

Discussion

Individual-specific model

If the pressure difference between outlet of the DAo and the three branches of the aortic arch (BA, LCCA, and LSCA) is properly, set as previously described, blood flow distribution of the DAo calculated by CFD and the distribution obtained from PC-MRI should show good correspondence. Conventional CFD analysis was performed with all outlet boundary conditions the same. In this study, outlet boundary conditions were determined based on blood flow distribution in the individual's DAo. CFD analysis based on individual-specific information provides more reliable results and allows us to estimate blood flow distribution of a newly developed vascular graft that has a nonconventional geometry. PC-MRI results showed that blood flow distribution into the DAo was approximately 70 % (Table 1). We examined the relationship between blood flow distribution into the DAo and energy loss (Fig. 6) (E_{loss}), which was calculated with the following equation:

$$E_{\text{loss}} = P_{\text{in}}Q_{\text{in}} - \sum(P_{\text{out}}Q_{\text{out}}) \quad (1)$$

where P_{in} is AAo total pressure, Q_{in} is AAo flow rate, P_{out} is Dao, BA, LCCA, and LSCA total pressure, and Q_{out} is DAo, BA, LCCA, and LSCA flow rate. Energy loss was the lowest at the point of 70–80 % blood flow distribution into the DAo. This suggests that the actual blood flow would properly reduce the load on the heart.

Blood flow distribution was calculated with *k*-epsilon analysis using individual-specific models. One calculation result, using *the k*-epsilon model, indicated that the right-side flow rate was 13.3 % and the left-side 14.9 % when blood flow distribution into the DAo was fixed at 71.9 %. On the other hand, results using the laminar flow model exhibited that only right-side flow was a slightly different value (13.2 %) and other values were the same as those with the *k*-epsilon model. Therefore, there was no significant difference in CFD results between laminar flow and *k*-epsilon models in our CFD analysis.

Evaluation of 4-branch models

Blood flow distribution in the 4-branch aslope model showed only 0.2 % difference from the benchmark model when the outlet boundary condition determined for the benchmark model was used for the aslope model. We concluded that the 4-branch model can be effectively used to analyze blood flow distribution when the three branches are placed at a 45° angle inclination from the top of the arch to the DAo.

Comparison of blood flow distribution between 4-branch and 3-branch graft

We analyzed the 3-branch graft blood flow distribution data to apply a determination of outlet boundary conditions for the 4-branch model. Blood flow distribution in the DAo of the 3-branch model was decreased by 5 %; right and left blood flow distribution measured by PC-MRI remained constant (Table 2), whereas it increased by 50 % in the right-side artery (BA) and decreased by 26 % in the left-side arteries (LCCA and LSCA). As shown above, the distribution of blood flow in the 3-branch model differs from that in

Table 2 Blood flow distribution of a 4-branch model and 3-branch model (%)

Model	Descending aorta	Right (BA)	Left (LCCA, LSCA)
4-Branch benchmark model	71.3	14.7	14.0
4-Branch aslope model	68.7	15.1	16.2
3-Branch model	67.7	21.2	11.1
3-Branch deformation model	77.6	8.6	13.8

BA brachiocephalic artery, *LCCA* left common carotid artery, *LSCA* left subclavian artery

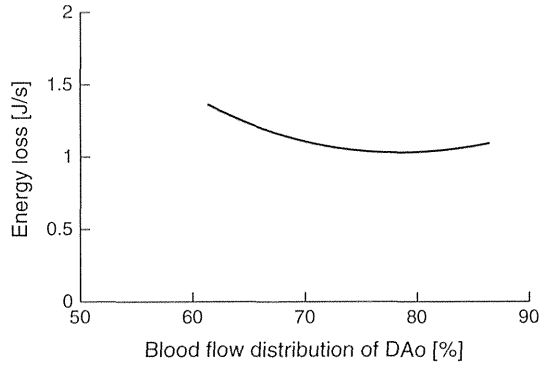

Fig. 6 Relationship between blood flow distribution into the descending aorta (DAo) and energy loss

the 4-branch aslope model. Distribution in such blood vessels is supposed to be affected by changes in the flow in the vessels, diameters of which are different from those in the natural system. In branch models, changes in these diameters could have an influence on flow distribution.

The distribution ratio of right to left by PC-MRI was about 1:1–1.4 in actual human individuals (Table 1), whereas similar results were obtained by 4-branch CFD with both (benchmark and aslope) models (Table 2). However, the distribution ratio of right to left was about 1:0.5 in a 3-branch model. The typical and maximum blood flow rates into brain tissue are 50 and 140 ml/min/100 g, respectively [13]. It is suggested that the 3-branch graft delivers more blood flow to the brain and upper limbs than does the 4-branch graft. Therefore, further study is required to survey the influence of the branch ratio of left to right on the brain blood flow. We determined the condition that coincides with the distribution in the DAo by PC-MRI using the benchmark model and studied blood flow distribution of total blood flow in the DAo and branches in the 3-branch graft model. The outlet pressure difference was 0.4 mmHg as the outlet boundary condition.

Usefulness of the new CFD method in the deformation model

We confirmed that a deformation in the graft significantly influenced blood flow distribution and that the CFD analysis could be useful before the graft is implanted. Expected difficulties can be modeled and analyzed before clinical application. This means that the influence of these expected difficulties pertaining to blood flow distribution of the 3-branch graft can be predicted. In this study, the aortic CFD model with a rigid wall was employed, and all analyses were done under steady and laminar flow. As there will be an effect of blood vessel compliance on blood flow distribution, validation of these assumptions will be performed by a mock circulatory system in our next study.

Conclusion

1. Blood flow distribution of the DAo in a healthy individual was 66–77 %.
2. Outlet boundary conditions can be determined using an individual-specific image model to establish a method to analyze blood flow distribution performance.
3. Outlet boundary conditions can be determined using a 4-branch benchmark model, and blood flow distribution of each model can be estimated.
4. Outlet boundary condition is given by a pressure difference between the DAo and the three branches of the aortic arch. As values of pressure difference (outlet boundary condition) in the individual-specific model and the 4-branch benchmark model are different, it is necessary to obtain more clinical data of healthy and diseased individuals in order to determine a reliable pressure difference.

Our method may be applied to estimate blood flow distribution of a newly developed vascular graft prior to its clinical use, thus providing useful information for safe use of the graft.

Acknowledgments This study was supported by a Grant-in-Aid for Challenging Exploratory Research from the Japan Society for the Promotion of Science. This work was aided by the project "Biomedical Engineering Research for Advanced Medical Treatment Using Nonclinical Study" of the Research Institute for Science and Engineering (08L01) of Waseda University.

References

1. Ohata T, Ueda H, Kobayashi K, et al. Terumo-Triplex grafts for total arch replacement: analysis of postoperative graft performance. J Artif Organs. 2012;15:240–3.

2. Galloway AC, Colvin SB, Grossi EA, et al. Surgical repair of type A aortic dissection by the circulatory arrest-graft inclusion technique in sixty-six patients. J Thorac Cardiovasc Surg. 1993; 105:781–8.
3. PMDA.2012. http://www.info.pmda.go.jp/ygo/pack/20800BZY00571000_B_07_01/. Accessed 1 Nov 2012.
4. PMDA.2012. http://www.info.pmda.go.jp/ygo/pack/20800BZY00571000_B_07_01/20800BZY00571000_B_07_01?view. Accessed 25 Oct 2012.
5. Chuter TA, Hiramoto JS, Chang C, et al. Branched stent-grafts: will these become the new standard? J Vasc Interv Radiol. 2008;19:S57–62.
6. Brinster DR. Simplified technique of total aortic arch replacement with minimal circulatory and myocardial ischemia. Ann Thorac Surg. 2012;94:e83–5.
7. Cires G, Noll RE Jr, Albuquerque FC Jr, et al. Endovascular debranching of the aortic arch during thoracic endograft repair. J Vasc Surg. 2011;53:1485–91.
8. Nakamura M, Wada S, Yokosawa S, et al. Measurement of blood flow in the left ventricle and aorta using clinical 2D cine phase-contrast magnetic resonance imaging. J Biomech Sci Eng. 2007; 2:46–57.
9. Lotz J, Meier C, Leppert A, et al. Cardiovascular flow measurement with phase-contrast MR imaging: basic facts and implementation. Radiographics. 2002;22:651–71.
10. Wen C-Y, Yang A-S, Tseng L-Y, et al. Investigation of pulsatile flowfield in healthy thoracic aorta models. Ann Biomed Eng. 2010;38:391–402.
11. Qian Y, Liu JL, Itatani K, et al. Computational hemodynamic analysis in congenital heart disease: simulation of the Norwood procedure. Ann Biomedcal Eng. doi:10.1007/s10439-010-9978-5.
12. Intech. http://www.intechopen.com/books/etiology-pathogenesis-and-pathophysiology-of-aortic-aneurysms-and-aneurysm-rupture/an-analysis-of-blood-flow-dynamics-in-aaa Accessed 25 Oct 2012.
13. Rushmer RF. Cardiovascular dynamics. 4th ed. Philadelphia: W. B. Saunders Company; 1961. p. 152.

止血戦略におけるフィブリノゲン製剤の役割

前田琢磨
Maeda Takuma
国立循環器病研究センター輸血管理室

Summary

大量出血症例では，初期から凝固障害が存在する可能性が高いにもかかわらず，救命や循環動態改善を優先し，まず，赤血球濃厚液輸血や晶質液，人工膠質液の大量投与がおこなわれるために，ますます希釈性，消費性凝固障害を増悪させている可能性がある．止血のためにフィブリノゲン製剤（クリオプレシピテートやフィブリノゲン濃縮製剤）を用いると輸血量が大幅に減少するという報告があいついでいる．今後わが国においてフィブリノゲン製剤が導入されれば，大量出血においてはまずフィブリノゲン製剤を投与という日がくる可能性もある．

Key Words

・大量出血　・フィブリノゲン製剤　・止血　・フィブリノゲン

はじめに

大量出血症例では，初期から凝固障害が存在する可能性が高いにもかかわらず，救命や循環動態改善を優先し，まず，赤血球濃厚液輸血や晶質液，人工膠質液の大量投与がおこなわれるために，ますます希釈性，消費性凝固障害を増悪させている可能性がある．また出血性ショックやそれに伴う低体温，アシドーシスなどが，さらに凝固障害を増悪させている[1]．フィブリノゲンは，凝固因子のなかでの最終基質であり，血液凝固のメカニズムの最終段階でフィブリン（不溶性の網状線維素）となり，血栓を形成することで，止血に大変重要な役割を果たしている．したがって，ほかの凝固因子が活性化されても，フィブリノゲンがなければ，止血機構が十分にはたらかないこととなる．また，大量出血時に，凝固因子のなかで一番早期に止血に必要な血中濃度（約100mg/dL）を保てなくなるという特性をもち[2]，出血による急性低フィブリノゲン血症にいかに対応するかが，大量出血を早期に止血する際の大変重要な課題であることが指摘されている．このため，米国の輸血ガイドライン，輸血アルゴリズムについて記載されている文献では，心臓血管外科手術の大量出血などで低フィブリノゲン血症をきたした場合，止血のためにフィブリノゲン製剤（クリオプレシピテートやフィブリノゲン濃縮製剤）の使用が推奨されている[3][4]が，わが国では一般化されていない．しかし，その必要性は長きにわたり叫ばれつづけている．

本稿では大量出血においてのフィブリノゲン製剤の効能をエビデンスにもとづいて解説し，大量出血におけるフィブリノゲン製剤を用いた戦略にも言及する．

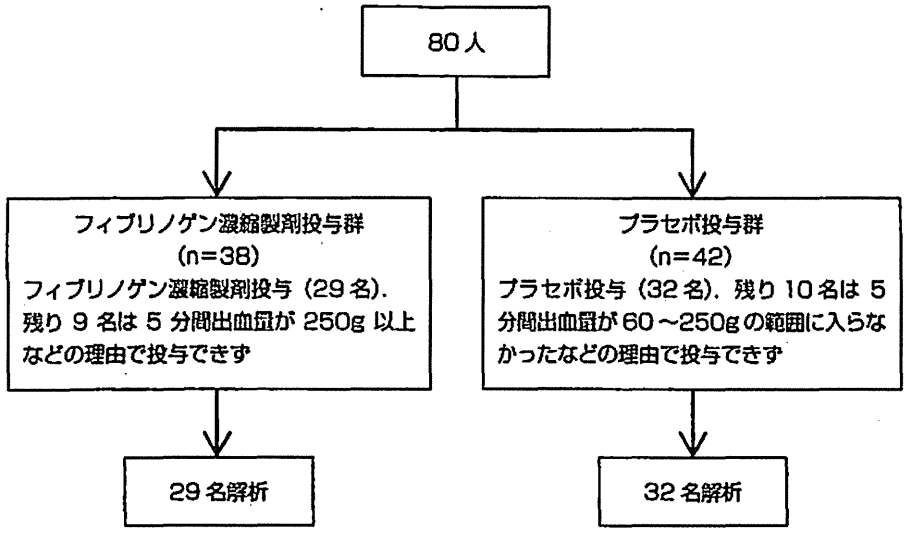

図❶ Hannover大学における二重盲検ランダム化比較試験
（Rahe-Meyer N *et al*, 2013[5]より引用）

1．大量出血への対応の鍵はフィブリノゲン補充にあり

2013年にドイツのHannover大学から衝撃的な論文が発表された[5]．この試験は一施設による18歳以上の人工心肺を用いた，胸部および胸腹部大動脈置換術を受けた患者に対し，人工心肺離脱後の5分間出血量が60～250gであった場合にフィブリノゲン濃縮製剤もしくは生理食塩水を投与するという二重盲検ランダム化比較試験である（図❶）．フィブリノゲン濃縮製剤投与群では平均8gのフィブリノゲンが投与されていた．驚くべきことに，フィブリノゲン濃縮製剤で介入した群では，同種血輸血が回避された割合は45％にも及ぶ一方で，プラセボ群において同種血輸血回避率は0％であった．さらに，術後24時間の総輸血量はプラセボ群と比較してフィブリノゲン濃縮製剤投与群で85％削減が認められた．この研究においては，血栓症や有害事象が増加していないかの検討もされているが，とくに有意な有害事象の増加はなかったとされる．

フィブリノゲン濃縮製剤については，後ろ向き研究ではあるものの，外傷の領域でも輸血頻度や患者予後改善につながるという報告もあり[6]，この領域においてもフィブリノゲン製剤に対する今後の動向が注目される．

2014年9月現在，わが国においては安全なフィブリノゲン濃縮製剤の供給が十分でなく，またクリオプレシピテートが供給されないことから，大量出血時にはフィブリノゲン上昇を目指して新鮮凍結血漿（fresh frozen plasma：FFP）が投与されることが多い．当院においては輸血部でクリオプレシピテートを作製しており，とくに大血管外科において積極的に使用している．図❷Aに示すように，FFP480を4℃で30時間程度かけて低温融解し，遠心分離するとフィブリノゲンが多く含まれる白い沈殿物を認めるが，これがクリオプレシピテートである．つづいて，おもにアルブミンなどが含まれる上清部分を無菌操作で別バックに移動させ（図❷B），残った20～50mLをフィブリノゲンが濃縮されたクリオプレシピテートとして出庫している．原料のFFPに含まれるフィブリノゲンに個人差があるため，フィブリノゲン濃縮製剤と違いばらつきが多少あるものの，3パック（FFP480×3本分）でおおむねフィブリノゲンは約2g程度含まれることになる．しかも容量としては3パックでせいぜい150mL程度なので，容量負荷なくすぐに投与できるので，大量出血時には重宝している．

今後，わが国においてフィブリノゲン製剤が導入されれば，輸血のストラテジーが大きく変わる可能性がある．

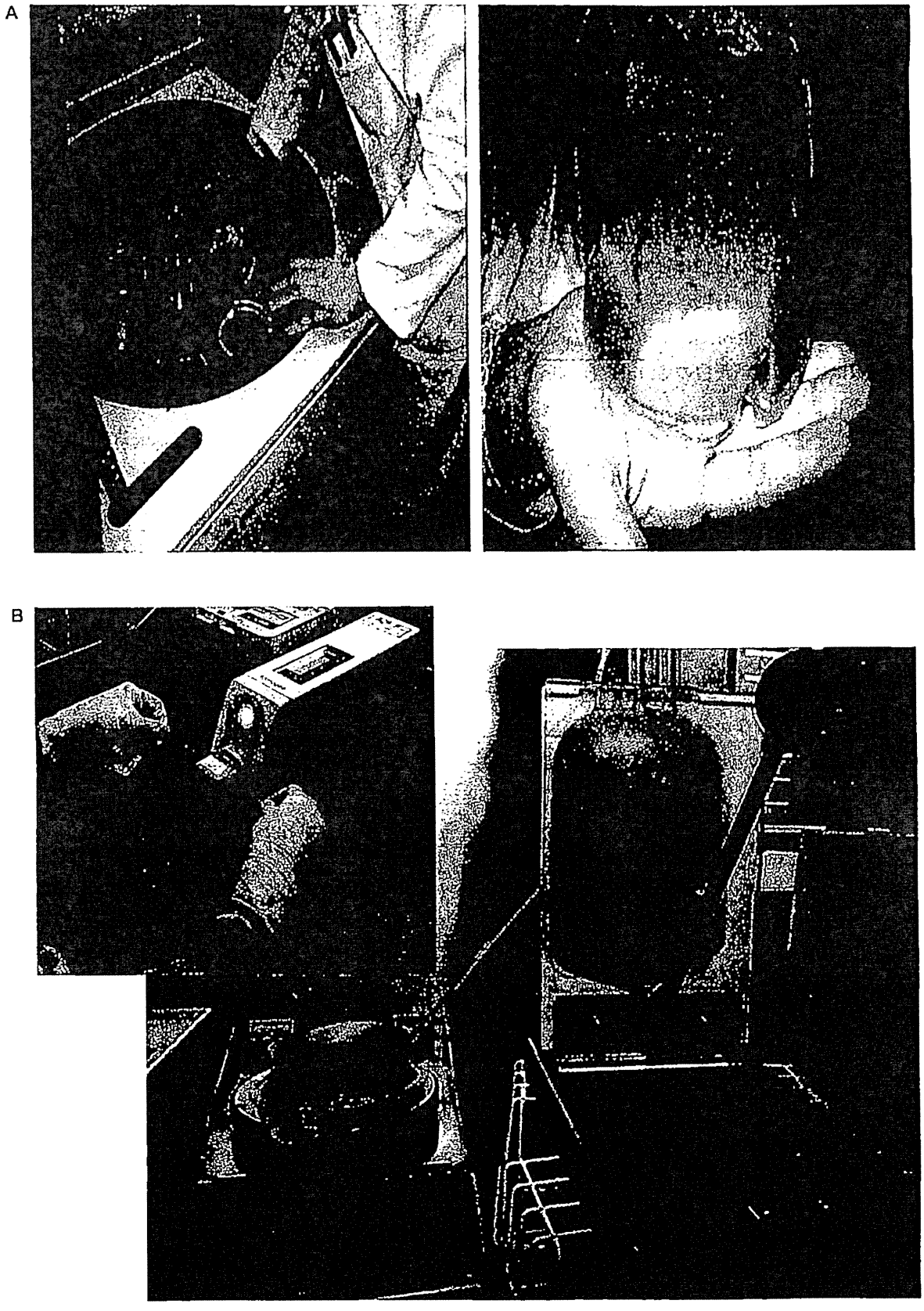

図❷ 当院におけるクリオプレシピテート作製の様子

2. 止血のメカニズム ～なぜフィブリノゲン高値が止血につながるか～

フィブリノゲン値が高いほうが止血によいのは感覚的には理解できるが，ここはおさらいの意味もふくめて，止血のメカニズムからその理由を紐解いていく．止血のメカニズムは一次止血と二次止血に区別できる．一次止血においては，外傷などで血管内皮細胞が破綻し，露出したコラーゲンに von Willebrand factor（vWF）が結合する．血小板は血小板膜糖蛋白の GPIb（glycoprotein Ib）受容体を介して vWF と結合し，血管内皮細胞下組織に粘着，凝集して血小板血栓ができる．粘着した血小板は形態を変え，従来の円盤状の形態から偽足を出した形態となる．活性化した血小板はさまざまな顆粒を放出，血小板表面には血小板膜糖蛋白の GPIIb/IIIa 受容体が発現される．この GPIIb/IIIa に対してフィブリノゲンが結合し，血小板血栓を強固にする．つまり，フィブリノゲンは二次止血だけでなく，一次止血にも重要なはたらきを担っているのである．このようにフィブリノゲンは血小板血栓の安定化につながっているので，高いフィブリノゲン量は，血小板数の低下を補正できる可能性も指摘されている[7]．

二次止血の舞台は，凝集した血小板のリン脂質に富んだ膜である．内因系にせよ，外因系にせよ，凝固カスケードにはこのリン脂質と凝固因子が関与し，最終的にはトロンビンが産生されて，フィブリノゲンがフィブリンになって血栓が完成する．このように，一次止血においても血小板血栓を強固にする意味と，二次血栓において最終基質として血栓を完成させるという二つの側面から，止血においてフィブリノゲン値が高いことは重要であることが分かる．

3. フィブリノゲン補充のカットオフ値は？

フィブリノゲン補充の目安として，多くのガイドラインで 100mg/dL があげられていることが多いが，じつはこの推奨についてのエビデンスレベルは低く，エキスパートオピニオンにもとづいている．しかしながら，このカットオフ値はじつは低すぎるのではないかという可能性が指摘されている．2013 年に出た報告[8]ではフィブリノゲン濃度 200mg/dL 未満群では大量輸血症例が増加していたとされる．（図❸）これは単施設後ろ向き観察研究で，人工心肺使用心臓手術 4,606 例を対象としている．フィブリノゲン濃度 200mg/dL 未満群は 42%の症例で，そのうち 18.9%が大量輸血を受けていた．一方，200mg/dL 以上群では 13.5%が大量輸血を受けていた（$p<0.0001$）．リスク因子を調整後でも，大量出血のオッズ比は，1.8（1.4～2.2）であり，傾向スコアを用いた解析でも 1.5（1.2～2.0）であったとされる．

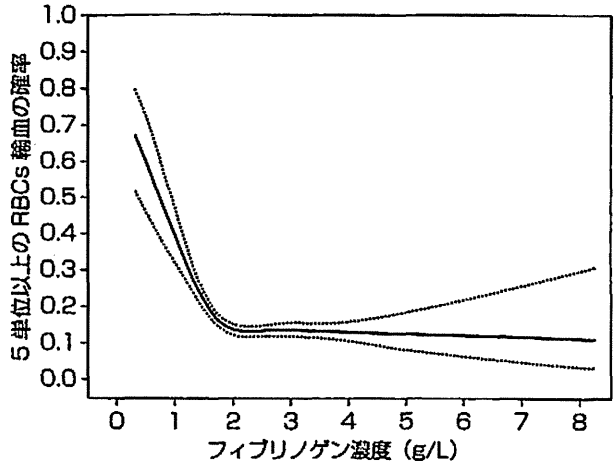

図❸ フィブリノゲン濃度と輸血量の関係
RBCs：red blood cells（赤血球）
（Karkouti K *et al*, 2013[8] より引用）

このほかにも，ドイツの Hannover 大学からの報告で，上行大動脈および大動脈弁置換術の患者を対象に，フィブリノゲン濃縮製剤を治療の最初に介入し，その後は輸血アルゴリズム（図❹）[9]に従うことで，総輸血量や術後出血量の大幅な減少が認められたとしているが，この試験においてはフィブリノゲン値が平均 200mg/dL 程の所でフィブリノゲン濃縮製剤が投与されている[9]．また，冠動脈バイパス術において出血を防ぐために必要なフィブリノゲン値は 100mg/dL よりずっと高いのではないかとする報告も散見されている[10]．麻酔科医の感

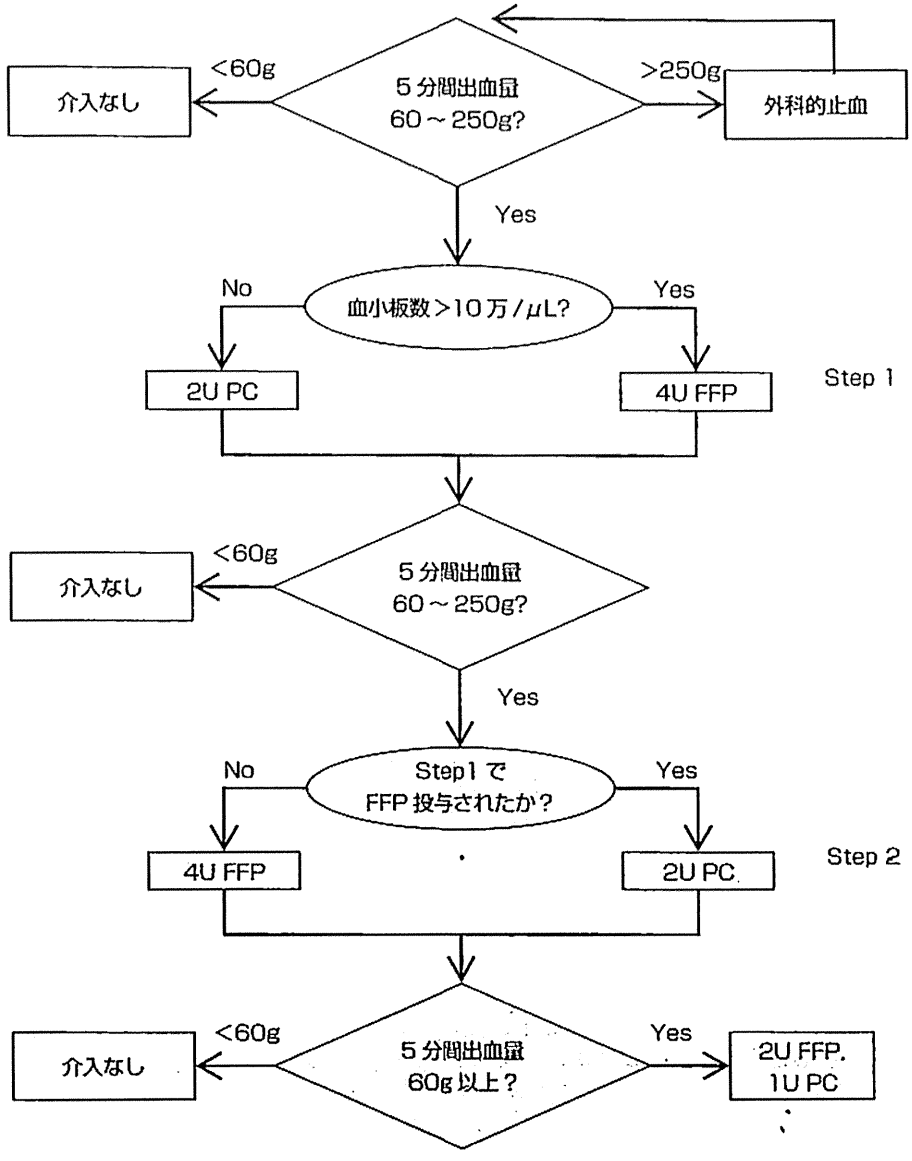

図❹ Hannover大学の報告におけるフィブリノゲン濃縮製剤介入後の輸血アルゴリズム
注）ドイツにおけるPC1U＝日本のPC約14単位
FFP：fresh frozen plasma（新鮮凍結血漿），PC：platelet concentrate（濃厚血小板）
（Rahe-Meyer N *et al*, 2009[9] より引用）

覚としてもフィブリノゲン補充のカットオフ値は100mg/dLよりは高いというのは頷けることではあるが，どれくらいが適切なのかについてはいまだに明確ではない．

4．これからの大量出血における戦略

大量出血において，早期から積極的にFFPや濃厚血小板を使えば出血量を減らし，患者予後を改善するという報告があいついでいる．イラク戦争において，外傷患者に赤血球濃厚液：FFP：濃厚血小板を1：1：1で投与することで，大量出血の患者の予後を改善したとの報

告[11]から，通常の外傷患者，またそれ以外の大量出血患者においてもこの考え方が拡大されてきている．しかしながら，この最適比に関しては明確な結論は出ていない．その理由として，大量出血の患者においてランダム比較試験をおこないにくいことがあげられる．したがって，さまざまなバイアスが入りやすく，たとえば生存バイアスの存在が指摘されている．つまり，死亡している患者にはFFPの投与量が少なかったので，FFPの使用が多いほうが予後がよいと結論付けられる．しかし，FFPは融解に時間がかかるために，大量出血で早期に死亡した患者には投与できないので，どうしても生存した患者にFFPが多く入りやすいのである．実際にこの生存バイアスは過去の論文[12]でも指摘され，この生存バイアスを除くため，時間経過を考慮し解析をおこなうと，死亡率とFFP：赤血球濃厚液は関係なかったとされる．

大量出血症例においてフィブリノゲンを補充することが出血を減らすということは，前述のHannover大学からの論文に代表されるように，大きな流れとなっている．したがって，今後わが国においてフィブリノゲン製剤が導入されれば，大量出血においてはまずフィブリノゲン製剤を投与という日がくる可能性もある．しかしながら，フィブリノゲン製剤の使用によって，深部静脈血栓症などの血栓症が増加する懸念もあり，フィブリノゲン製剤を新規の効果的な止血剤として使用することには慎重な意見もある[7]ことを付け加えておきたい．

おわりに

2014年9月現在，フィブリノゲン濃縮製剤と生理食塩水の国際共同多施設二重盲検プラセボ対照ランダム比較試験であるREPLACE study（Randomized Evaluation of fibrinogen versus PLACEbo in complex cardiovascular surgery）の症例登録が終了し，解析待ちの状況である．これは人工心肺使用大動脈置換術患者を対象とし，フィブリノゲン濃縮製剤または生理食塩水で介入し，総輸血量や治験薬投与後24時間以内の同種血輸血量の比較をおこなうものであるが，この治験によりフィブリノゲン濃縮製剤の有効性が示されれば，わが国においてもフィブリノゲン製剤の薬事承認が得られる可能性があり，大量出血における輸血のストラテジーに大きな変化をもたらすと思われる．今後の動向に注目したい．

文献

1) Sihler KC *et al*：Massive transfusion：new insights. *Chest* **136**：1654-1667, 2009
2) Hiippala ST *et al*：Hemostatic factors and replacement of major blood loss with plasma-poor red cell concentrates. *Anesth Analg* **81**：360-365, 1995
3) Hardy JF：Endpoints in clinical trials on transfusion requirements：the need for a structured approach. *Transfusion* **45**（1 Suppl）：9S-13S, 2005
4) Despotis G *et al*：A review of transfusion risks and optimal management of perioperative bleeding with cardiac surgery. *Transfusion* **48**（1 Suppl）：2S-30S, 2008
5) Rahe-Meyer N *et al*：Effects of fibrinogen concentrate as first-line therapy during major aortic replacement surgery：a randomized, placebo-controlled trial. *Anesthesiology* **118**：40-50, 2013
6) Levy JH *et al*：Fibrinogen and hemostasis：a primary hemostatic target for the management of acquired bleeding. *Anesth Analg* **114**：261-274, 2012
7) Sørensen B *et al*：A critical evaluation of cryoprecipitate for replacement of fibrinogen. *Br J Haematol* **149**：834-843, 2010
8) Karkouti K *et al*：The relationship between fibrinogen levels after cardiopulmonary bypass and large volume red cell transfusion in cardiac surgery：an observational study. *Anesth Analg* **117**：14-22, 2013
9) Rahe-Meyer N *et al*：Bleeding management with fibrinogen concentrate targeting a high-normal plasma fibrinogen level：a pilot study. *Br J Anaesth* **102**：785-792, 2009
10) Karlsson M *et al*：Plasma fibrinogen level, bleeding, and transfusion after on-pump coronary artery bypass grafting surgery：a prospective observational study. *Transfusion* **48**：2152-2158, 2008
11) Borgman MA *et al*：The ratio of blood products transfused affects mortality in patients receiving massive transfusions at a combat support hospital. *J Trauma* **63**：805-813, 2007
12) Snyder CW *et al*：The relationship of blood product ratio to mortality：survival benefit or survival bias? *J Trauma* **66**：358-362；discussion 362-364, 2009

▷第60回学術集会
シンポジウム14：危機的出血(大量出血・大量輸血)におけるチーム医療(4)◁

危機的出血に対する臨床検査部門の対応

河 原 好 絵*1 渡 辺 愉 美*2 友 田 豊*3 紀 野 修 一*4

Contribution of Central Hospital Laboratory to Critical Bleeding

Yoshie KAWAHARA *1, *Yumi WATANABE**2,
*Yutaka TOMODA**3 and *Shuichi KINO*, MD, PhD*4

It has been reported that fibrinogen products, such as fibrinogen concentrates, cryoprecipitate (CRYO), and fresh frozen plasma, are beneficial for treating coagulopathy due to massive blood transfusion. For the appropriate use of these products, it is necessary to evaluate the status of coagulopathy and determine the trigger level of the fibrinogen concentration for the administration of fibrinogen products.

In our institution, we established a treatment procedure for coagulopathy due to massive transfusion in 2011. This procedure includes determination of the trigger level for administration of CRYO (150 mg/dL), timing of sample collection for the evaluation of coagulation parameters (prothrombin time, activated partial thromboplastin time, and fibrinogen) and concentration status during the operation, and a method for rapid coagulation testing (turnaround time within 15 minutes) in critical bleeding.

Since 2011, we have performed 56 rapid coagulation tests for patients suffering from critical bleeding. The average turnover time was 13 minutes. According to the rapid coagulation test results, CRYO was administered to 27 patients. These results are satisfactory for treating critical bleeding patients.

We stress the need for the establishment of a rapid coagulation test system in the central hospital laboratory. 【Review】

[Rinsho Byori **62** : 1286～1294, 2014]

Corresponding author: *Yoshie KAWAHARA*, Department of Medical Laboratory and Blood Center, Asahikawa Medical University Hospital, Asahikawa 078-8510, Japan. E-mail: kawahara@asahikawa-med.ac.jp

【Key Words】 critical bleeding(危機的出血), cryoprecipitate: CRYO(クリオプレシピテート), fibrinogen(フィブリノゲン), coagulation test(凝固検査), turnaround time: TAT(所要時間)

危機的出血時には大量の輸液および輸血により体内の血漿成分が希釈され，希釈性凝固障害が惹き起こされる。この希釈性凝固障害に対応するためには，失われた凝固因子の中でも特にフィブリノゲンの補充が必要であり，クリオプレシピテート(以下，クリオ製剤)やフィブリノゲン製剤投与の有用性が報告されている[1)2)]。しかし，それらの使用には基準が示されておらず，適正使用のためにも各施設においてマニュアルが整備され，使用基準が明確化される必要がある。

当院では2011年11月よりクリオ製剤の供給を開始している。供給開始にあたって院内マニュアルを

*1～4旭川医科大学病院臨床検査・輸血部(〒078-8510 旭川市緑が丘東2条1-1-1)